

Discriminating and Imaging Different Phosphatidylcholine Species within Phase-Separated Model Membranes by Principal Component Analysis of TOF-Secondary Ion Mass Spectrometry Images

Bita Vaezian,[†] Christopher R. Anderton,[‡] and Mary L. Kraft^{*,†}

Departments of Chemical and Biomolecular Engineering and Chemistry, University of Illinois at Urbana–Champaign, Urbana, Illinois 61801, United States

Time-of-flight secondary ion mass spectrometry (TOF-SIMS) enables chemically imaging the distributions of various lipid species in model membranes. However, discriminating the TOF-SIMS data of structurally similar lipids is very difficult because the high intensity, low mass fragment ions needed to achieve submicrometer lateral resolution are common to multiple lipid species. Here, we demonstrate that principal component analysis (PCA) can discriminate the TOF-SIMS spectra of four unlabeled saturated phosphatidylcholine species, 1,2-dilauroyl-sn-glycero-3-phosphocholine (DLPC), 1,2-dimyristoyl-sn-glycero-3-phosphocholine (DMPC), 1,2-dipalmitoyl-sn-glycero-3-phosphocholine (DPPC), and 1,2-distearoyl-sn-glycero-3-phosphocholine (DSPC) according to variations in the intensities of their low mass fragment ions ($m/z \leq 200$). PCA of TOF-SIMS images of phase-separated DSPC/DLPC and DPPC/DLPC membranes enabled visualizing the distributions of each phosphatidylcholine species with higher contrast and specificity than that of individual TOF-SIMS ion images. Comparison of the principal component (PC) scores images to atomic force microscopy (AFM) images acquired at the same membrane location before TOF-SIMS analysis confirmed that the PC scores images reveal the phase-separated membrane domains. The lipid composition within these domains was identified by projection of their TOF-SIMS spectra onto PC models developed using pure lipid standards. This approach may enable the identification and chemical imaging of structurally similar lipid species within more complex membranes.

Comprehensive characterization of lipid mixing behavior within model lipid membranes provides valuable information on how lipid–lipid interactions may contribute to cell membrane organization and function.^{1,2} The biophysical and structural properties of model lipid membranes are routinely probed using fluorescence

microscopy and atomic force microscopy.^{3–7} Spatially resolved compositional information that complements this biophysical and structural data is also essential for understanding biological membrane organization but is presently more difficult to acquire. The lipid distribution within model membranes can be imaged in a chemically specific manner using secondary ion mass spectrometry (SIMS).^{8–20} However, additional advances in SIMS methodologies are necessary to improve the specificity, sensitivity, and lateral resolution of lipid identification and imaging in label-free systems.

Time-of-flight SIMS (TOF-SIMS) is a molecular imaging technique that reveals the chemical composition at the surface of

- (2) Veatch, S. L.; Keller, S. L. *Biochim. Biophys. Acta* **2005**, *1746*, 172–185.
- (3) Wesolowska, O.; Michalak, K.; Maniewska, J.; Hendrich, A. B. *Acta Biochim. Polonica* **2009**, *56*, 33–39.
- (4) Crane, J. M.; Tamm, L. K. In *Methods in Membrane Lipids*; Dopico, A. M., Ed.; Humana Press Inc.: Totowa, NJ, 2007; Vol. 400, pp 481–488.
- (5) Galush, W. J.; Nye, J. A.; Groves, J. T. *Biophys. J.* **2008**, *95*, 2512–2519.
- (6) Johnston, L. J. *Langmuir* **2007**, *23*, 5886–5895.
- (7) Seantier, B.; Giocondi, M.-C.; Grimellic, C. L.; Milhiet, P.-E. *Curr. Opin. Colloid Interface Sci.* **2008**, *13*, 326–337.
- (8) Leufgen, K. M.; Rulle, H.; Benninghoven, A.; Sieber, M.; Galla, H. J. *Langmuir* **1996**, *12*, 1708–1711.
- (9) McQuaw, C. M.; Sostarecz, A. G.; Zheng, L.; Ewing, A. G.; Winograd, N. *Langmuir* **2005**, *21*, 807–813.
- (10) McQuaw, C. M.; Zheng, L.; Ewing, A. G.; Winograd, N. *Langmuir* **2007**, *23*, 5645–5650.
- (11) Saleem, M.; Galla, H.-J. *Biochim. Biophys. Acta Biomembr.* **2010**, *1798*, 730–740.
- (12) Sostarecz, A. G.; McQuaw, C. M.; Ewing, A. G.; Winograd, N. *J. Am. Chem. Soc.* **2004**, *126*, 13882–13883.
- (13) Bourdos, N.; Kollmer, F.; Benninghoven, A.; Ross, M.; Sieber, M.; Galla, H.-J. *Biophys. J.* **2000**, *79*, 357–369.
- (14) Breitenstein, D.; Batenburg, J. J.; Hagenhoff, B.; Galla, H.-J. *Biophys. J.* **2006**, *91*, 1347–1356.
- (15) Zheng, L.; McQuaw, C. M.; Ewing, A. G.; Winograd, N. *J. Am. Chem. Soc.* **2007**, *129*, 15730–15731.
- (16) Popov, J.; Vobornik, D.; Coban, O.; Keating, E.; Miller, D.; Francis, J.; Petersen, N. O.; Johnston, L. J. *Langmuir* **2008**, *24*, 13502–13508.
- (17) Galli Marquer, C.; Kraft, M. L.; Weber, P. K.; Hutcheon, I. D.; Boxer, S. G. *Biophys. J.* **2005**, *88*, 2965–2975.
- (18) Kraft, M. L.; Fishel, S. F.; Galli Marquer, C.; Weber, P. K.; Hutcheon, I. D.; Boxer, S. G. *Appl. Surf. Sci.* **2006**, *252*, 6950–6956.
- (19) Kraft, M. L.; Weber, P. K.; Longo, M. L.; Hutcheon, I. D.; Boxer, S. G. *Science* **2006**, *313*, 1948–1951.
- (20) Anderton, C. R.; Weber, P. K.; Lou, K.; Hutcheon, I. D.; Kraft, M. L. *Biochim. Biophys. Acta* **2010**, DOI: 10.1016/j.bbamem.2010.09.1016.

* Corresponding author. E-mail: mlkraft@illinois.edu.

[†] Department of Chemical and Biomolecular Engineering.

[‡] Department of Chemistry.

(1) Feigenson, G. W. *Biochim. Biophys. Acta* **2009**, *1788*, 47–52.

a sample with as high as submicrometer lateral resolution.^{11,21,22} For the analysis of lipid membranes using TOF-SIMS, lipid components are usually identified according to a limited number of characteristic lipid fragment ions in the mass spectra, such as those corresponding to lipid headgroups, fatty acids, and backbone segments.^{10,12–16,23,24} However, the use of these types of fragment ions to discriminate between structurally similar lipids, such as different phosphatidylcholine species, is especially problematic. Though low molecular weight fragment ions (i.e., phosphocholine and hydrocarbon ions) generate sufficient ion yields to achieve submicrometer lateral resolution, these ions are common to many structurally similar lipid species, prohibiting their use for species identification. Molecular ions and large fragment ions may be unique to a single component, but they usually have very low yields that compromise the working lateral resolution of the resulting TOF-SIMS image.^{14,25} Structurally similar lipids can be endowed with characteristic fragment ions through the use of stable isotope labeling,^{14,16–20,24,25} but label-free approaches are desired to facilitate sample preparation and SIMS analysis of native cell membranes.

Principal component analysis (PCA) is a multivariate analysis technique that is used to identify linear combinations of multiple mass peaks that reveal similarities and differences in the TOF-SIMS data acquired from different samples.^{26,27} Because PCA distinguishes the spectra according to variations in the relative intensities of many TOF-SIMS mass peaks, the abundant low mass ions that are common to structurally similar molecules, and thus, not utilized for univariate spectra interpretation, can be exploited for component identification.²⁷ This use of a larger fraction of the TOF-SIMS mass peaks for component identification increases image contrast and improves the specificity of component identification.^{26–29} The TOF-SIMS spectra of structurally similar molecules, including monosaccharide stereoisomers,³⁰ proteins,^{31–33} and alkane thiols,³⁴ have been successfully discriminated using PCA. PCA has also been used to identify unlabeled lipids with different head groups and deuterated lipids in model membranes by their TOF-SIMS data.^{25,28} However, successfully discriminating the TOF-SIMS data from unlabeled structurally similar lipid species (i.e., lipids with the same head groups and degrees of saturation in the fatty acid tails) using PCA has not been reported.

- (21) Walker, A. V. *Anal. Chem.* **2008**, *80*, 8864–8870.
- (22) Williams, P. J. *Biol.* **2006**, *5*, 18.
- (23) Sostarecz, A. G.; Cannon, D. M., Jr.; McQuaw, C. M.; Sun, S.; Ewing, A. G.; Winograd, N. *Langmuir* **2004**, *20*, 4926–4932.
- (24) Gunnarsson, A.; Kollmer, F.; Sohn, S.; Hook, F.; Sjovall, P. *Anal. Chem.* **2010**, *82*, 2426–2433.
- (25) Biesinger, M. C.; Miller, D. J.; Harbottle, R. R.; Possmayer, F.; McIntyre, N. S.; Petersen, N. O. *Appl. Surf. Sci.* **2006**, *252*, 6957–6965.
- (26) Pachuta, S. J. *Appl. Surf. Sci.* **2004**, *231*–*232*, 217–223.
- (27) Graham, D. J.; Wagner, M. S.; Castner, D. G. *Appl. Surf. Sci.* **2006**, *252*, 6860–6868.
- (28) Biesinger, M. C.; Paeppegaey, P.-Y.; McIntyre, N. S.; Harbottle, R. R.; Petersen, N. O. *Anal. Chem.* **2002**, *74*, 5711–5716.
- (29) Tyler, B. J.; Rayal, G.; Castner, D. G. *Biomaterials* **2007**, *28*, 2412–2423.
- (30) Berman, E. S. F.; Kulp, K. S.; Knize, M. G.; Wu, L.; Nelson, E. J.; Nelson, D. O.; Wu, K. J. *Anal. Chem.* **2006**, *78*, 6497–6503.
- (31) Wagner, M. S.; Shen, M.; Horbett, T. A.; Castner, D. G. *J. Biomed. Mater. Res.* **2003**, *64A*, 1–11.
- (32) Wagner, M. S.; Tyler, B. J.; Castner, D. G. *Anal. Chem.* **2002**, *74*, 1824–1835.
- (33) Wagner, M. S.; Shen, M.; Horbett, T. A.; Castner, D. G. *Appl. Surf. Sci.* **2003**, *203*–*204*, 704–709.
- (34) Graham, D. J.; Ratner, B. D. *Langmuir* **2002**, *18*, 5861–5868.

Here, we investigate the ability to distinguish and image structurally similar lipids within supported lipid membranes using PCA to interpret TOF-SIMS images. Because high mass ions have low intensities in the spectra acquired from lipid membranes with TOF-SIMS, we first evaluate the feasibility of discriminating four different unlabeled saturated phosphatidylcholine species that are frequently studied in model membranes, 1,2-dilauroyl-*sn*-glycero-3-phosphocholine (DLPC), 1,2-dimyristoyl-*sn*-glycero-3-phosphocholine (DMPC), 1,2-dipalmitoyl-*sn*-glycero-3-phosphocholine (DPPC), and 1,2-distearoyl-*sn*-glycero-3-phosphocholine (DSPC), by PCA of the low mass ions ($m/z \leq 200$) in the TOF-SIMS data. Discrimination of these lipid species by TOF-SIMS is especially challenging because each contains a phosphocholine headgroup, glycerol backbone, and two saturated fatty acid tails that differ only in length (12, 14, 16, and 18 carbons per fatty acid in DLPC, DMPC, DPPC, and DSPC, respectively). Next, we assess whether each lipid species within supported lipid membranes composed of DSPC/DLPC and DPPC/DLPC can be differentiated, visualized, and chemically identified by PCA of TOF-SIMS images. These lipid mixtures were selected because they are known to phase separate into DLPC-rich fluid-phase domains and DSPC- or DPPC-rich gel-phase domains at room temperature.^{19,20,35,36} In addition, the chemically specific SIMS imaging of the lipid organization within these membranes has only been accomplished using stable isotope labeling.^{19,20} To evaluate whether the principal component (PC) scores images generated from the TOF-SIMS images of the phase-separated membranes show the sizes and shapes of the gel- and fluid-phase domains, we compare the PC scores images to atomic force microscopy (AFM) images of the phase-separated domains that were acquired at the same membrane locations prior to TOF-SIMS analysis. Finally, we investigate whether the lipid composition at these distinct locations can be identified by projecting their TOF-SIMS data onto PC models developed using spectra from lipid standards.

MATERIALS AND METHODS

Preparation of Thin Films of Pure Phosphatidylcholine Lipids. DLPC, DMPC, DPPC, and DSPC were purchased in chloroform from Avanti Polar Lipids (Alabaster, AL) and used without further purification. A thin film of each lipid standard was created by spotting a small droplet of the lipid dissolved in chloroform onto a 5 mm × 5 mm silicon substrate that was patterned with a chrome grid to facilitate sample positioning.¹⁹ For each lipid standard, three different samples were prepared on different days. The sample was subjected to vacuum for a minimum of 3 h to evaporate the solvent.

Preparation of Phase-Separated Supported Lipid Membranes. The lipid mixtures used to create phase-separated supported lipid membranes consisted of a 1:2 molar ratio of DSPC/DLPC or DPPC/DLPC, plus 1 mol % of the fluorescent lipid, 1-palmitoyl-2-[12-(7-nitro-2-1,3-benzodiazol-4-yl)amino]lauroyl-*sn*-glycero 3-phosphocholine (NBD-PC, Avanti Polar Lipids, Alabaster, AL) for visualization with fluorescence microscopy. Small unilamellar vesicles (SUVs) composed of DSPC/DLPC/NBD-PC were prepared by tip sonification (Branson Tip

- (35) Mabrey, S.; Sturtevant, J. M. *Proc. Natl. Acad. Sci. U.S.A.* **1976**, *73*, 3862–3866.
- (36) Feigenson, G. W.; Bulbantz, J. T. *Biophys. J.* **2001**, *80*, 2775–2788.

Sonifier Model 250D, Branson Ultrasonics, Danbury, CT).^{20,37} SUVs composed of DPPC/DLPC/NBD-PC were made with an extruder^{17,19,37} because this method produced larger phase-separated domains. Supported lipid membranes were formed by slow-cooled vesicle fusion onto the silicon substrates described above.^{19,20,37} The DSPC/DLPC and DPPC/DLPC bilayers were annealed at 70 and 55 °C, respectively, for 1 h, and then were slowly cooled at a rate of 2.6 and 1.5 °C/h, respectively, to induce phase separation.

To permit analyzing the samples with TOF-SIMS, which is performed under ultrahigh vacuum (UHV), the samples were flash-frozen in liquid ethane, and then, the ice was sublimed from the bilayer using an oil-free scroll pump (Triscroll 300, Varian, Inc. Palo Alto, CA).¹⁹ Fluorescence microscopy (Leica DM6000 B, Q-Imaging EXi Blue Fluorescence Microscope) was used to evaluate membrane quality and to generate optical maps of the samples that enabled imaging the same sample locations with both AFM and TOF-SIMS.

AFM Analysis of Phase-Separated Lipid Membranes. The freeze-dried supported lipid membranes were imaged with an Asylum MFP-3D Stand Alone AFM (Asylum Research, Santa Barbara, CA) in ambient air and temperature. Measurements were taken in AC mode (tapping) in the repulsive tip–sample interaction regime with standard 300 kHz AFM probes (Tap300Al-G, Budget Sensors, Bulgaria). AFM images were flattened to the second-order, and line scans between the gel- and surrounding fluid-phase domains were made to verify that symmetric phase-separated domains were present.

TOF-SIMS Analysis. TOF-SIMS analysis was performed on a PHI Trift-III TOF-SIMS (Physical Electronics Incorporated, Chanhassen, MN) using a gold liquid ion gun operated at 22 kV. A ¹⁹⁷Au⁺ primary ion beam with 3.7 and 1 nA was used to analyze the lipid films and phase-separated lipid membranes, respectively. TOF-SIMS data from the lipid films were acquired from 100 μm × 100 μm sample regions using bunched mode. TOF-SIMS spectra were acquired at four different regions on each pure lipid film.

TOF-SIMS analysis of the phase-separated supported lipid membranes was performed in unbunched mode for optimal lateral resolution. TOF-SIMS images with 256 pixels × 256 pixels were acquired from 85 μm × 85 μm or 65 μm × 65 μm areas on the membrane and were cropped to show subregions of the membrane. TOF-SIMS spectra were obtained with a mass range of 0–800 amu and a mass resolution of $M/\Delta M = 850$ at the C₃H₇⁺ peak (m/z 43). The analysis time varied according to the size of the acquisition area in order to keep a constant primary ion dose of 2.4×10^{12} ions/cm² for the pure lipid films and 2.8×10^{13} ions/cm² for the phase-separated supported lipid membranes.

PCA of TOF-SIMS Spectra of Pure Lipid Films and Phase-Separated Lipid Membranes. PCA was performed using the PLS Toolbox and the MIA Toolbox (v.5.2.2 and v.1.0.7, respectively, Eigenvector Research, Manson, WA), which were run in MATLAB (v.7.8.0, MathWorks Inc., Natick, MA). Unit mass binning was applied to each spectrum acquired from a pure lipid film. The mass peaks from m/z 30 to 200 were used for analysis,

but the peaks with m/z of 39 (potassium), 40 (calcium), 41 (hydrocarbon contaminant), 52 (chrome grid), 73 (PDMS contaminant), and 147 (PDMS contaminant) were removed from the spectra.³⁸ The TOF-SIMS data was arranged in a matrix such that the different samples formed the rows and the individual mass peaks formed the columns. Each mass spectrum of a pure lipid film was normalized to the total intensity of the selected peaks and mean-centered. A PC model was constructed using the mass spectra from the four different lipid species. Score plots were generated that illustrate the projection of the TOF-SIMS data from the phosphatidylcholine species onto the new PCs. Loading plots were created that exhibit the linear combination of mass peaks that contributed to each PC. Mass peaks with large positive or negative loadings on a PC tend to have relatively higher intensities in the normalized spectra of the samples with positive or negative scores, respectively, on the same PC.³⁴

For PCA of the TOF-SIMS images acquired on the phase-separated supported lipid membranes, the mass peaks with counts of at least 0.1% of the highest observed count rate were imported directly into the PLS toolbox. The intensities of the mass peaks were summed over 2 pixels × 2 pixels, producing downbinned images with 128 pixels × 128 pixels. If the chrome grid that is used for sample positioning was visible in the TOF-SIMS image, PCA was performed only on the region of the image where the membrane was located. As in the analysis of the lipid standards, the mass peaks listed above (m/z 0 to 29, 39, 40, 41, 52, 73, and 147) were removed from the spectra. The resulting spectra were normalized to the total intensity of the selected peaks and autoscaled. Finally, a PC model was created that converted the TOF-SIMS data from n ion images of 128 pixels × 128 pixels, where n is the number of mass peaks, into a two-dimensional array with n columns and 16 384 rows that contained the TOF-SIMS data collected at every pixel. A score value was calculated for each pixel, and the data was reassembled into a 128 pixels × 128 pixels image in which the score value at each pixel was encoded by a pseudocolor scale. We refer to this graphic representation of the scores values as a PC scores image. A loading plot for each PC that shows the linear combination of mass peaks that contribute to the PC was generated.

Calculation of Image Contrast. To compare the quality of the individual TOF-SIMS images and PC scores images, contrast between the gel- and fluid-phase membrane domains within the images was calculated according to eq 1, as previously reported.^{29,39}

$$c_{\text{gel,fluid}} = \frac{|I_{\text{gel}} - I_{\text{fluid}}|}{\sigma_{\text{gel,fluid}}} \quad (1)$$

where I_{gel} is the average intensity in the gel-phase domains, I_{fluid} is the average intensity in the fluid-phase domains, and $\sigma_{\text{gel,fluid}}$ is the standard deviation of the intensity within both regions. Intensity refers to counts in the individual TOF-SIMS ion images and to the PC score values in the PC scores images.

Identification of Lipid Composition in the Gel- and Fluid-Phase Domains within Phase-Separated Membranes using PCA. TOF-SIMS data were extracted from 12 regions of interest (ROIs) on the gel- and fluid-phase membrane regions, which were

(37) Lin, W. C.; Blanchette, C. D.; Ratto, T. V.; Longo, M. L. *Biophys. J.* **2006**, 90, 228–237.

(38) Oran, U.; Unveren, E.; Wirth, T.; Unger, W. E. S. *Appl. Surf. Sci.* **2004**, 227, 318–324.
(39) Tyler, B. J. *Appl. Surf. Sci.* **2006**, 252, 6875–6882.

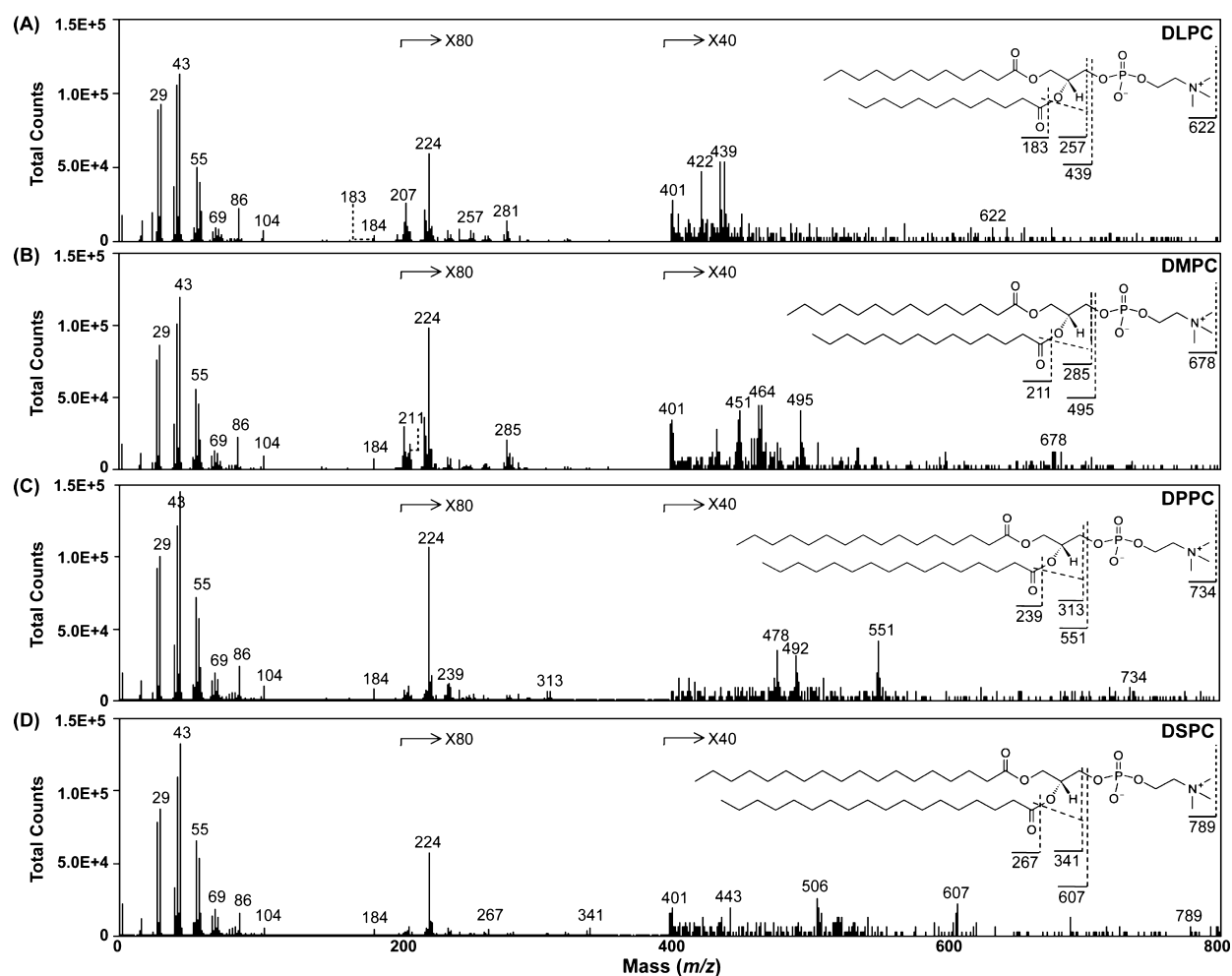


Figure 1. TOF-SIMS positive-ion spectrum and structures (inset) of four different saturated phosphatidylcholine species: (A) DLPC, (B) DMPC, (C) DPPC, and (D) DSPC. The spectra were obtained using an ion dose of 2.4×10^{12} ions/cm².

identified by comparison to the AFM image of the DSPC/DLPC and DPPC/DLPC membranes (24 ROIs per membrane, 48 ROIs in total). Unit mass binning was applied to each spectrum acquired from a ROI on the membrane. For each of the resulting 48 TOF-SIMS spectra, the normalized peaks from m/z 30 to 200 that did not correspond to the impurity peaks listed above were loaded as the validation block in the PC model developed using the pure lipid films. The mass spectra from the lipid membranes were arranged in a matrix as described above, normalized to the total intensity of the selected peaks for each spectrum, mean-centered, and then projected onto the PC model developed using the pure lipid films. Although the spectra from the lipid standards were acquired with higher mass resolution than the TOF-SIMS images of the phase-separated lipid membranes, the mass resolution in the data set was ultimately limited by the unit mass binning applied to all the spectra prior to data processing.

RESULTS AND DISCUSSION

PCA Discrimination of TOF-SIMS Spectra of Saturated Phosphatidylcholine Species. Representative TOF-SIMS positive ion mass spectra of four saturated phosphatidylcholine species are shown in Figure 1. The unique mass peaks that could be used to discriminate DLPC, DMPC, DPPC, and DSPC include the molecular ions (m/z 622, 678, 734, and 789, respectively),

diacylglycerol fragment ions (m/z = 439, 495, 551, and 607, respectively), monoacylglycerol fragment ions (m/z = 257, 285, 313, and 341, respectively), and fatty acids (m/z = 183, 211, 239, 267, respectively). However, high molecular weight ions ($m/z > 200$), including many of the aforementioned fragment ions, usually have low intensities in the TOF-SIMS spectra acquired from supported lipid membranes,^{10,16,24} though new primary ion sources may enhance the intensities of high mass fragment ions.⁴⁰ Few characteristic mass peaks with $m/z \leq 200$ are present in the spectra of the lipid standards due to their similar structures.

PCA was performed using the mass peaks with m/z from 30 to 200, excluding known contaminants, because these ions ($m/z \leq 200$) are relatively abundant in the TOF-SIMS positive-ion spectra of lipid membranes.^{10,24} The resulting PC scores plot of the lipid spectra projected onto PC1 and PC2 (Figure 2A) demonstrates that these phosphatidylcholine species can be differentiated and classified. The ellipse around each group in the scores plot shows the 95% confidence limit for the boundary of the group.⁴¹ The ellipse outlined with a dotted blue line represents the border for the entire PC model at the 95% confidence limit. The majority of the variation between lipid species is captured by PC1, which separates the lipids according to the lengths of their

(40) Johansson, B. *Surf. Interface Anal.* 2006, 38, 1401–1412.

(41) Wagner, M. S.; Castner, D. G. *Langmuir* 2001, 17, 4649–4660.

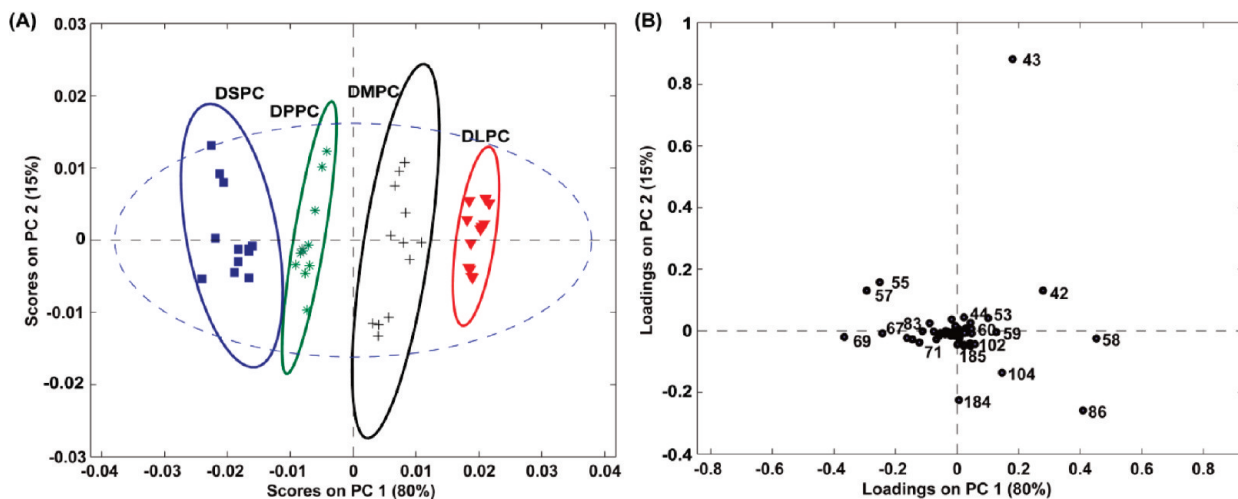


Figure 2. Scores and loadings plots from PCA of the TOF-SIMS positive-ion spectra of DLPC, DMPC, DPPC, and DSPC lipid films. These four saturated phosphatidylcholine species differ only in the lengths of their fatty acid tails. (A) The scores plot on PC1 and PC2 differentiates the four phosphatidylcholine lipid species. (B) The loadings plot illustrates the positive ion mass peaks that contribute to the variation captured by each PC. PCA was performed on the ion peaks with m/z from 30 to 200 amu, excluding the potassium (m/z = 39), calcium (m/z = 40), hydrocarbon impurity (m/z = 41), chrome (m/z = 52), and PDMS contaminant (m/z = 73 and 147) peaks. These peaks were normalized to the total counts obtained over this mass range and mean-centered. The ellipses in the score plot that are outlined with a solid line represent the border for each group at the 95% confidence limit. The ellipse outlined with a dotted blue line represents the border for the entire PC model at the 95% confidence limit.

Table 1. Information on Select Peaks in the TOF-SIMS Positive Ion Spectra of DLPC, DMPC, DPPC, and DSPC

m/z	assignment ^{14,28,42,43}	comments	loadings on PC1
30	CH_4N^+ or C_2H_6^+	head group or hydrocarbon fragment	0.044
43	C_3H_7^+ or $\text{C}_2\text{H}_2\text{O}^+$	hydrocarbon chain or fatty acid fragment	0.181
55	C_4H_7^+	hydrocarbon chain fragment	-0.251
57	C_4H_9^+	hydrocarbon chain fragment	-0.293
58	$\text{C}_3\text{H}_8\text{N}^+$	head group fragment	0.452
59	$\text{C}_3\text{H}_9\text{N}^+$	head group fragment	0.127
67	C_5H_7^+	hydrocarbon chain fragment	-0.243
69	C_5H_9^+	hydrocarbon chain fragment	-0.366
71	$\text{C}_5\text{H}_{11}^+$	hydrocarbon chain fragment	-0.122
72	$\text{C}_4\text{H}_{10}\text{N}^+$	head group fragment	0.010
74	$\text{C}_4\text{H}_{12}\text{N}^+$	head group fragment	0.044
79	C_6H_7^+	hydrocarbon chain fragment	-0.112
81	C_6H_9^+	hydrocarbon chain fragment	-0.145
83	$\text{C}_6\text{H}_{11}^+$	hydrocarbon chain fragment	-0.163
86	$\text{C}_5\text{H}_{12}\text{N}^+$	head group fragment	0.409
95	$\text{C}_7\text{H}_{11}^+$	hydrocarbon chain fragment	-0.059
97	$\text{C}_7\text{H}_{13}^+$	hydrocarbon chain fragment	-0.054
102	$\text{C}_5\text{H}_{12}\text{NO}^+$	choline	0.058
104	$\text{C}_5\text{H}_{14}\text{NO}^+$	choline	0.146
150	$\text{C}_5\text{H}_{13}\text{NPO}_2^+$	head group fragment	0.022
166	$\text{C}_5\text{H}_{13}\text{NPO}_3^+$	head group fragment	0.022
183	$\text{C}_{12}\text{H}_{23}\text{O}^+$	dodecanoic acid fragment	0.024
184	$\text{C}_5\text{H}_{15}\text{NPO}_4^+$	phosphocholine	0.006

fatty acid tails. The mass peaks responsible for this lipid-specific separation have high loadings on PC1 and are shown in the loading plot (Figure 2B). These values are partially tabulated in Table 1. Both hydrocarbon and headgroup fragments have large loadings on PC1, indicating the normalized intensities of these ions vary significantly between the phosphatidylcholine species. The hydrocarbon ions with m/z of 55 (C_4H_7^+), 57 (C_4H_9^+), 67 (C_5H_7^+), 69 (C_5H_9^+), 71 ($\text{C}_5\text{H}_{11}^+$), 79 (C_6H_7^+), 81 (C_6H_9^+), and 83 ($\text{C}_6\text{H}_{11}^+$)^{28,42} have negative loadings on PC1 and, therefore, relatively higher normalized intensities in the spectra from DSPC and DPPC. Head group fragments with m/z of 58 ($\text{C}_3\text{H}_8\text{N}^+$), 59 ($\text{C}_3\text{H}_9\text{N}^+$), 86 ($\text{C}_5\text{H}_{12}\text{N}^+$), 102 ($\text{C}_5\text{H}_{12}\text{NO}^+$), 104 ($\text{C}_5\text{H}_{14}\text{NO}^+$), 166

($\text{C}_5\text{H}_{13}\text{NPO}_3^+$), and 184 ($\text{C}_5\text{H}_{15}\text{NPO}_4^+$)^{14,28,43} and the dodecanoic acid fragment at m/z = 183 load positively on PC1 and, thus, have relatively higher normalized intensities in the spectra of DMPC and DLPC. Although all four lipid species have the same phosphocholine headgroup, the headgroup ions have a relatively higher normalized intensity in the spectra of DLPC and DMPC, likely because DLPC and DMPC have shorter fatty acid tails that contribute fewer hydrocarbon ions to their spectra. On PC2, the loadings for the mass peaks that correspond to lipid head groups (m/z = 184, 166, 104, 86, and 58) are negative, and the small hydrocarbon ion at m/z = 43 has a large positive loading. PC2 may separate the samples according to disparities in their surface

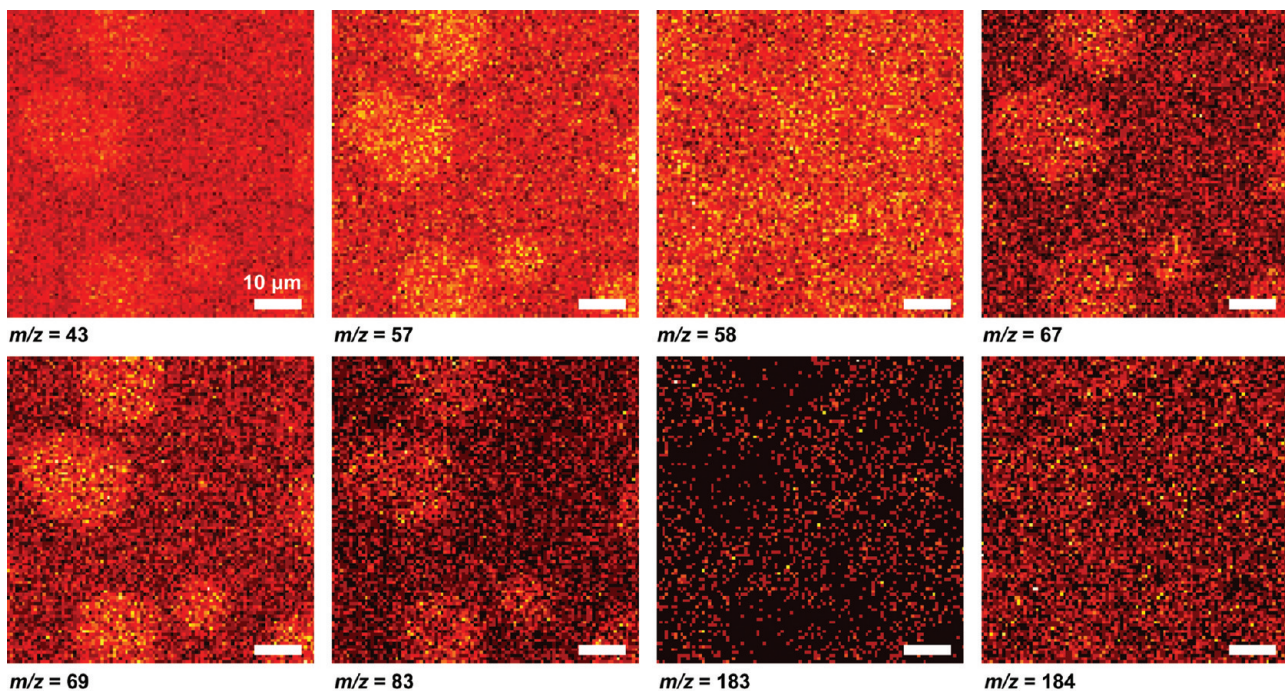


Figure 3. Select TOF-SIMS positive ion images acquired on phase-separated supported lipid membranes composed of DSPC/DLPC (1:2 molar ratio) show the intensity of the specified mass peak. The images were obtained in an unbunched mode for optimal lateral resolution. The TOF-SIMS images were acquired of a $85\text{ }\mu\text{m} \times 85\text{ }\mu\text{m}$ area with 256 pixels \times 256 pixels, downbinned to 128 pixels \times 128 pixels, and cropped to show a $65\text{ }\mu\text{m} \times 65\text{ }\mu\text{m}$ area of the membrane.

coverage, as opposed to lipid-specific chemical variations, because the intensities of the higher mass fragment ions and low mass hydrocarbon ions are influenced by surface coverage to differing degrees.⁴⁴ This ability to discriminate the lipid spectra according to the relative intensities of their low mass ions suggests that PCA of TOF-SIMS images might enable discriminating and imaging saturated phosphatidylcholine species within phase-separated lipid membranes.

PCA of TOF-SIMS Images of Phase-Separated Supported Lipid Membranes. Typically, TOF-SIMS analysis is performed using an ion dose below 10^{13} ions/ cm^2 to prevent exceeding the static limit.^{28,45} However, our initial studies demonstrated that analysis within the static limit yielded insufficient counts to visualize the lipid domains with PCA (Figure S1, Supporting Information). Instead, we obtained higher ion counts and better contrast and sensitivity in the resulting PC scores images by slightly exceeding the static limit. Therefore, we used an ion dose of 2.8×10^{13} ions/ cm^2 to image the phase-separated lipid membranes. To further improve the image quality, the TOF-SIMS images were downbinned to 128 pixels \times 128 pixels. Figure 3 shows select TOF-SIMS ion images of a DSPC/DLPC membrane (1:2 molar ratio). For comparison, the AFM image acquired at the same membrane location prior to TOF-SIMS analysis is shown in Figure 4A. In the AFM image, the DSPC-rich gel-phase domains have diameters between 5 and $25\text{ }\mu\text{m}$ (light gray regions, Figure 4A) and protrude $\sim 1.5\text{ nm}$ above the surrounding DLPC-rich fluid-phase regions (dark gray

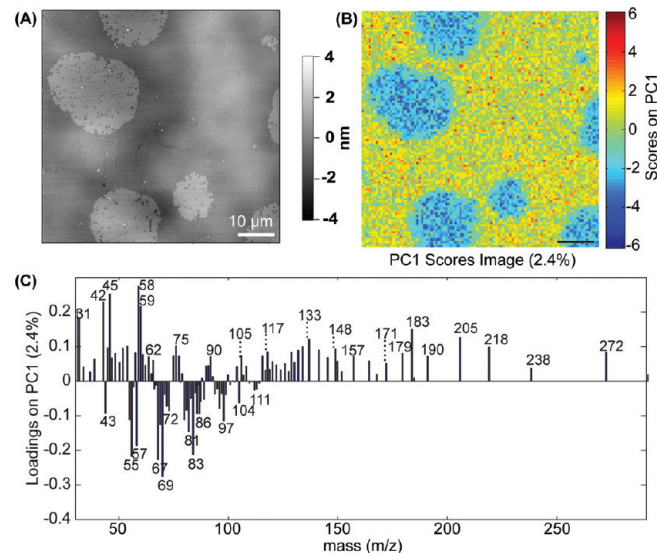


Figure 4. (A) AFM image shows gel- and fluid-phase domains that are enriched with DSPC and DLPC, respectively, in the DSPC/DLPC (1:2 molar ratio) membrane. (B) The PC1 scores images generated by PCA of the downbinned TOF-SIMS image of the same membrane location. The gel-phase domains have negative scores (blue), and the fluid-phase locations have positive scores (green, yellow, and red). (C) The loadings on PC1 show the mass peaks with the largest variability between the gel- and fluid-phase regions of the membrane. The mass peaks with positive loadings have higher normalized intensities on the fluid-phase DLPC-rich regions, and the peaks with negative loading have elevated normalized intensities on the gel-phase DSPC-rich domains.

(44) Bourdos, N.; Kollmer, F.; Benninghoven, A.; Sieber, M.; Galla, H.-J. *Langmuir* 2000, 16, 1481–1484.

(45) Harbottle, R. R.; Nag, K.; McIntyre, N. S.; Possmayer, F.; Petersen, N. O. *Langmuir* 2003, 19, 3698–3704.

areas, Figure 4A). This height difference is slightly smaller than that previously measured between gel- and fluid-phase domains

Table 2. Contrast Calculated for the Individual TOF-SIMS Ion Images (Figure 3) and PC Scores Image (Figure 4B) of the Same Region of a Phase-Separated DSPC/DLPC Membrane

image	contrast
<i>m/z</i> 43	1.13
<i>m/z</i> 57	1.10
<i>m/z</i> 58	0.45
<i>m/z</i> 67	1.00
<i>m/z</i> 69	1.23
<i>m/z</i> 83	0.90
<i>m/z</i> 183	0.40
<i>m/z</i> 184	0.18
PC1	1.97

in DSPC/DLPC membranes,^{19,20,37} which may be due to our use of a repulsive tip–sample interaction for AFM imaging.^{46,20,47} Submicrometer-size fluid-phase subdomains were also detected by AFM within the gel-phase domains.

Comparison between the AFM and TOF-SIMS ion images of the same membrane location indicates the hydrocarbon fragments with *m/z* of 43 ($C_3H_7^+$), 57 ($C_4H_9^+$), 67 ($C_5H_7^+$), 69 ($C_5H_9^+$), and 83 ($C_6H_{11}^+$) have higher counts (Figure 3) and normalized intensities (Figure S2, Supporting Information) on the gel-phase DSPC-rich domains. In contrast, the ions with *m/z* of 58 ($C_3H_8N^+$) and 183 ($C_{12}H_{23}O^+$) have higher counts (Figure 3) and normalized intensities (Figure S2, Supporting Information) on the fluid-phase DLPC-rich regions. These observations are fairly consistent with the PC1 loadings calculated for the TOF-SIMS data from the pure lipid films (Figure 2B). Although the PC model of the pure lipid films indicates the relative normalized intensity of the phosphocholine ion (*m/z* = 184) is higher on DLPC, the contrast in the *m/z* = 184 ion image is too low to identify the phase-separated membrane domains. PCA of the TOF-SIMS images yielded PC scores images that graphically show the score value at every pixel in the TOF-SIMS image (Figure 4B). Comparison of the PC1 scores image to the AFM image acquired at the same location (Figure 4A) confirms that the PC1 scores image reveals phase separation in the membrane. The fluid-phase regions that are enriched with DLPC have positive scores (green, yellow, and red areas), and the gel-phase domains that are enriched with DSPC have negative scores (blue regions). The contrast values for the PC1 scores image (Figure 4B) and the individual TOF-SIMS ion images (Figure 3) were calculated as previously reported^{29,39} and are tabulated in Table 2. The higher contrast values of the PC scores image confirms that the PC1 scores image reveals the phase-separated lipid domains with better contrast than that obtained in the individual TOF-SIMS ion images. Therefore, although PC1 accounts for only 2.4% of the pixel-to-pixel variation in the normalized TOF-SIMS peak intensities, this variation is significant. The improvement in the sensitivity and specificity of lipid detection obtained with PCA is further demonstrated by the detection of the ~5 μ m-wide gel-phase domain at the top right corner of the AFM and PC1 scores images (Figure 4A), as this domain was not visible in any of the individual TOF-SIMS ion images (Figure 3). However, the submicrometer-size fluid-phase subdomains entrapped within the large gel-phase domains that

are shown in the AFM image (Figure 4A) were not resolved in the PC1 scores image. These domains were also not detectable in the PC scores images produced by PCA of the unbinned (256 pixels \times 256 pixels) TOF-SIMS data (Figure S3, Supporting Information), which indicates these features were smaller than the lateral resolution of the TOF-SIMS analysis.

The plot of the loadings on PC1 (Figure 4C) shows which mass peaks have large positive loadings and, therefore, higher normalized intensities on the fluid-phase DLPC-rich areas and peaks with large negative loadings and, thus, higher normalized intensities on the gel-phase DSPC-rich domains. Many of the mass peaks that correspond to DSPC and DLPC according to the PC model developed on the pure lipid films are correlated with the DSPC-rich gel-phase and DLPC-rich fluid-phase domains, respectively, based on the PC1 loadings for the PC model of the phase-separated membrane. This agreement suggests PC1 separates the spectra according to differences in lipid composition and not variations in lipid packing or topography. Furthermore, sample topography is not a likely source of the spectral variation captured by PC1 because the loadings for the phase-separated membrane have both positive and negative values, and topographic effects in TOF-SIMS images are often isolated on a single PC that primarily loads in a single direction.²⁶

We investigated the generality of PCA of TOF-SIMS spectra to discriminate and image different saturated phosphatidylcholine species by applying this approach to phase-separated DPPC/DLPC (1:2 molar ratio) membranes. Unlike the individual TOF-SIMS ion images of the DSPC/DLPC membrane (Figure 3), the domains are barely discernible in the TOF-SIMS images of the counts and normalized intensities of specific ions acquired from the DPPC/DLPC membrane (Figure 5 and Figure S4, Supporting Information). For comparison, the AFM image acquired at the same location prior to TOF-SIMS analysis (Figure 6A) shows gel-phase domains that are several micrometers in diameter and protrude ~1 nm above the surrounding fluid phase. This height difference is slightly smaller than that previously reported (1.4 nm),⁴⁸ which, as stated above, is likely due to our use of a repulsive tip–sample interaction for AFM imaging.^{46,20,47} Submicrometer-size gel-phase domains are also visible within the fluid phase.

The PC1 scores image (Figure 6B) clearly shows distinct regions that correlate with the gel- and fluid-phase domains detected with AFM (Figure 6A). Calculation of the contrast values, which are listed in Table 3, confirms that the contrast between the compositionally distinct gel- and fluid-phase domains is higher in the PC1 scores image than the individual TOF-SIMS ion images that are shown in Figure 5. Again, the submicrometer-size gel-phase domains that are visible in the AFM image (Figure 6A) were not resolved in either the downbinned or unbinned PC1 scores images (Figure 6B and S5, Supporting Information), indicating these domains are likely smaller than the lateral resolution of the TOF-SIMS analysis. The plot of the PC1 loadings shows the mass peaks that have negative loadings and, therefore, higher normalized intensities on the gel-phase DPPC-rich domains and the peaks with positive loadings and, thus, higher normalized intensities on the fluid-phase DLPC-rich domains (Figure 6C). Again the presence of both positive and negative loadings on PC1

(46) Schneider, J.; Dufrêne, Y. F.; Barger, W. R., Jr.; Lee, G. U. *Biophys. J.* 2000, 79, 1107–1118.

(47) Moraille, P.; Badia, A. *Langmuir* 2003, 19, 8041–8049.

(48) Tokumasu, F.; Jin, A. J.; Feigenson, G. W.; Dvorak, J. A. *Biophys. J.* 2003, 84, 2609–2618.

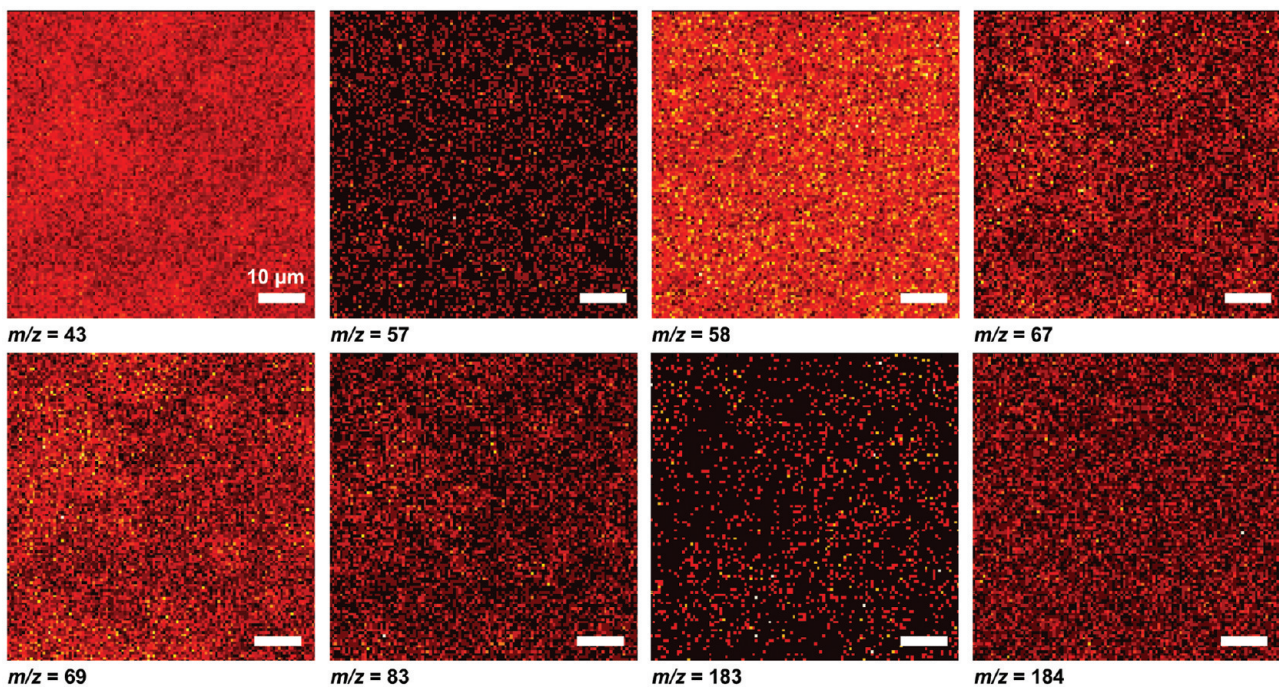


Figure 5. Select TOF-SIMS positive-ion images acquired on phase-separated supported lipid membranes composed of DPPC/DLPC (1:2 molar ratio) show the intensity of the specified mass peak. The images were obtained in unbunched mode for optimal lateral resolution. The TOF-SIMS images were acquired of a $65\text{ }\mu\text{m} \times 65\text{ }\mu\text{m}$ area with 256 pixels \times 256 pixels, downbinned to 128 pixels \times 128 pixels, and cropped to show a $60\text{ }\mu\text{m} \times 60\text{ }\mu\text{m}$ region of interest. Phase-separated domains are barely visible in these images.

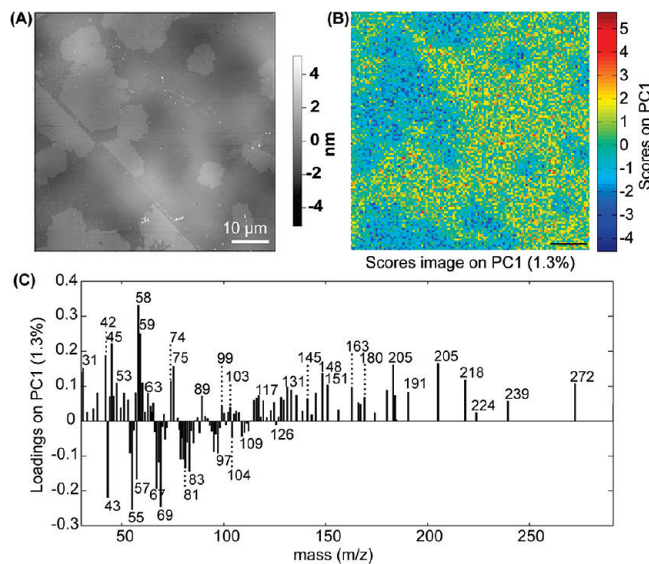


Figure 6. (A) AFM image shows the morphologies of the DPPC-enriched gel-phase domains and the surrounding DLPC-enriched fluid-phase regions in the DPPC/DLPC (1:2 molar ratio) phase-separated membrane. (B) PC1 scores image created by PCA of the downbinned TOF-SIMS data of the same membrane location as (A). The gel-phase domains have negative scores (blue), and the fluid-phase locations have positive scores (green, yellow, and red). (C) Loadings on PC1 show the mass peaks with the largest variability between the gel- and fluid-phase membrane regions. Mass peaks with negative loadings have higher normalized intensities on the DPPC-rich gel-phase regions, and positives loadings have higher normalized intensities on the DLPC-rich fluid-phase domains.

indicates topography is not likely responsible for the spectral variation captured by PC1.

Table 3. Contrast Calculated for the Individual TOF-SIMS Ion Images (Figure 5) and PC Scores Image (Figure 6B) of the Same Region of a Phase-Separated DPPC/DLPC Membrane

image	contrast
m/z 43	0.66
m/z 57	0.55
m/z 58	0.28
m/z 67	0.55
m/z 69	0.64
m/z 83	0.43
m/z 183	0.26
m/z 184	0.04
PC1	1.31

Determination of Lipid Composition within Distinct Membrane Domains by Projection onto the PC Model of Lipid Standards. To identify the lipid composition within the gel- and fluid-phase domains (Figure 4B and 6B), we projected the TOF-SIMS data that we extracted from regions corresponding to gel- or fluid-phase domains in the DSPC/DLPC and DPPC/DLPC membranes onto the PC model developed using the DLPC, DMPC, DPPC, and DSPC spectra, which was shown in Figure 2. The resulting PC scores plot is shown in Figure 7. The PC1 scores for the TOF-SIMS spectra acquired from the DSPC/DLPC membrane designate that the gel-phase domains correspond to DSPC, in agreement with phase diagrams and previous reports.^{19,20,35,36} The fluid-phase regions had scores on PC1 that were most similar to DMPC, followed by DLPC. Because these are model membranes with known composition, we conclude that the fluid-phase domains were enriched with DLPC and not DMPC. We suggest the lower scores on PC1 may be due to the presence of tiny gel-phase domains in the fluid phase. The scores on PC1 for the spectra acquired on the DPPC/

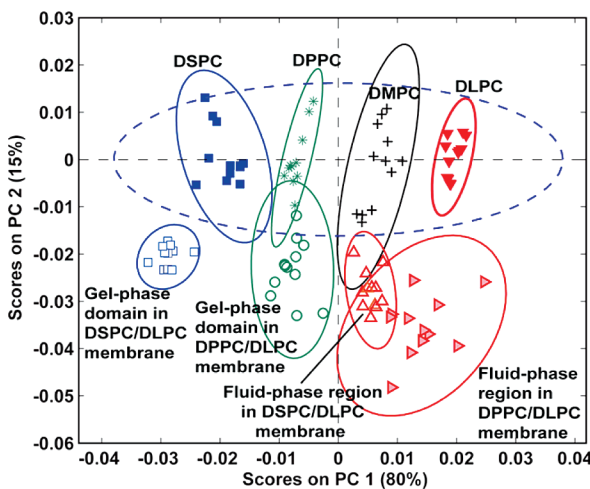


Figure 7. Projection of the TOF-SIMS data extracted from gel- and fluid-phase regions of the DSPC/DLPC and DPPC/DLPC membrane onto the PC scores plot developed using the positive-ion spectra of the four phosphatidylcholine species: DLPC, DMPC, DPPC, and DSPC. The PC1 scores of the TOF-SIMS data extracted from the phase-separated membranes identifies the lipid composition at these sites.

DLPC membrane indicate that the gel-phase domains are composed of DPPC, as expected from the phase diagrams for this lipid mixture.^{19,20,35,36} The fluid-phase regions of the DPPC/DLPC membrane had PC1 scores that were consistent with both DLPC and DMPC. Again, because the sample did not contain DMPC, we conclude that the fluid-phase membrane regions were enriched with DLPC. We speculate that tiny gel-phase domains were present within the fluid-phase regions that had lower scores on PC1. The agreement between the compositions we determined by projecting onto PC models developed using lipid standards and previous reports^{19,20,35,36} suggests the chemical variations identified in the PC scores images were not due to the presence of the small amount (1 mol %) of fluorophore-labeled lipid in the fluid phase or difference in lipid packing between the two phases. We note that the spectra from the lipid membranes had large residuals on the PC model of the lipid standards, indicating the lipid membranes were not well described by this PC model. This imperfect fit may be due to differences in the surface coverage,

lipid orientation, or ion dose used to analyze the lipid standards and membranes and suggests these conditions should be kept constant to optimize the fit. Nonetheless, these results demonstrate that the lipid composition within distinct membrane domains can be identified through the use of PC models developed using spectra from lipid standards.

CONCLUSIONS

The distributions of saturated phosphatidylcholine species within phase-separated lipid membranes can be differentiated and visualized by slightly exceeding the static limit of TOF-SIMS analysis and using PCA to interpret the TOF-SIMS images. Projection of the TOF-SIMS data from phase-separated domains onto PC models of pure lipid samples enables the identification of the lipid composition within subregions of the membrane. This method can be used to image and identify the lipid composition at small areas within label-free model membranes composed of less well-characterized lipid mixtures. The development of PC models constructed using the spectra from additional lipid species and cholesterol may also allow the discrimination and chemical imaging of structurally similar lipids within more complex membranes. Further improvements in TOF-SIMS imaging and multivariate analysis approaches may also permit the detection of submicrometer-sized membrane domains.

ACKNOWLEDGMENT

M.L.K. holds a Career Award at the Scientific Interface from the Burroughs Wellcome Fund. Portions of this work were carried out in the Frederick Seitz Materials Research Laboratory Central Facilities, Univ. of Illinois, which are partially supported by the U.S. Department of Energy (DOE) under Grants DE-FG02-07ER46453 and DE-FG02-07ER46471.

SUPPORTING INFORMATION AVAILABLE

Additional information as noted in text. This material is available free of charge via the Internet at <http://pubs.acs.org>.

Received for review June 22, 2010. Accepted November 2, 2010.

AC101640C